FLUCOME 2009
10th International Conference on Fluid Control, Measurements, and Visualization
August 17–21, 2009, Moscow, Russia

# A STUDY ON FLOW BEHAVIOR INSIDE A SIMPLE MODEL OF EJECTOR

Taketoshi Koita [1] and Junjiro Iwamoto [2]

## ABSTRACT

This paper is concerned with the experimental results on the internal flow of the ejector. To improve the ejector effect and vacuum performance, it is important to clarify the flow behavior within the ejector. In this study a simple rectangular model of ejector is used to obtain the flow pattern in the ejector. The internal flow of the ejector is visualized by shadowgraph and schlieren methods and the stagnation pressure of the secondary flow is measured to investigate the ejector performance with and without the secondary flow rate. It is found how flow behavior of the ejector influences the ejector performance.

**Keywords: Ejector, Supersonic flow, Ejector performance, Shock wave, Shear layer**

## INTRODUCTION

An air ejector consists of a primary supersonic driving nozzle, a converging section, a mixing section, and a diffuser. In the ejector system when the high-pressure primary jet is emitted from the supersonic nozzle, the secondary fluid is entrained in a converging section from the atmosphere by reduction in pressure around the exit of the primary nozzle and shear action between the primary and secondary fluids. This phenomenon is called the ejector effect. So, it can draw the secondary fluid into the ejector, and the pressure of the mixed air of primary and secondary fluid increases in the diffuser, the mixed air being discharged into the atmosphere. Accordingly, the ejector is used to entrain the atmosphere in the ejector mode of combined cycle engine in the work by Tani *et al.* (2007) and as a compressor, e.g. a compressor in the refrigeration system in the work by Yamada and Nishijima (2008). When the entrance to the passage for the secondary flow is closed, ejector operates as vacuum pump. Thus, it can be used to lift some industrious products by vacuum and carry them to another place without using hand. The ejector performance depends on the configurations of the ejector and the pressure of the primary fluid. For a long time a variety of the configurations of the ejector have been studied to improve the ejector performance by experiment as shown in the work by Watanabe *et al.* (1956) and Matsuo *et al.* (1982) and numerical analysis. To improve the ejector performance it is very important to understand the internal fluid behavior in detail. Behavior of internal flow in vacuum ejector has been analyzed by hydraulic analogy and

[1] Graduate School of Engineering, Tokyo Denki University, 2-2 Kanda Nishiki-Cho, Chiyoda-Ku, Tokyo 101-8457, Japan, e-mail: 08gmm08@ms.dendai.ac.jp
[2] Department of Mechanical Engineering, Tokyo Denki University,2-2 Kanda Nishiki-Cho, Chiyoda-Ku, Tokyo 101-8457, Japan, e-mail: iwamoto@cck.dendai.ac.jp

numerical analysis as shown in the work by Endo *et al.* (2005). However, the visualization study on the internal flow of air ejector has not much been studied so far. In addition, the ejector configuration is different in different studies, so that the optimal configuration is not well established.

Therefore in this study a simple rectangular model of two-dimensional air ejector is used to obtain the flow pattern in the ejector. Under the conditions whether there is secondary flow or not, the internal flow of the ejector is visualized by shadowgraph and schlieren methods, and the secondary flow rate and the stagnation pressure of the secondary fluid are measured to investigate the ejector effect and the vacuum performance, and the experimental results are discussed and examined.

## EXPERIMENTAL CONSIDERATION

### Ejector Model

Figure 1 shows the ejector model in this study. The rectangular model is employed to obtain basic flow pattern in the ejector, primarily to understand the mixing action of primary jet and secondary air. The convergent nozzle is used, where the nozzle height is $d$ = 3 mm and the width 25 mm (aspect ratio 8.33). The inner radius of the nozzle is 20 mm. In order to obtain the basic flow pattern in the present experiment, the convergent section where the two streams mix, throat and diffuser are made of rectangular tube of uniform cross section, its height being $w$ = 10 mm and its width 25 mm (it is called ejector throat in the present study). The breadth of the port $s$ through which secondary fluid flows is varied as $s/d$ = 0.5, 1.0 and 1.5 to change the secondary flow rate. The length of the ejector throat $l$ and the breadth of the port $s$ are known to be important as the compression is the highest when $(l + s) / w$ = 6.45 in the experiment made by Watanabe *et al.* (1956) and 7 to 8 by Kastner and Spooner (1950). In the present experiment $l + s$ = 120 mm: i.e. $(l + s) / w$ = 12 to measure the static pressure of this ejector throat and discuss the ejector performance as a compressor in the future. The breadth of the secondary flow passage is $b$ = 12 mm, and the pipe connected to this passage whose diameter is $D$ = 18 mm has larger cross-sectional area than that of the secondary flow passage. Both side walls of ejector are made of quartz glass so as to visualize the internal flow.

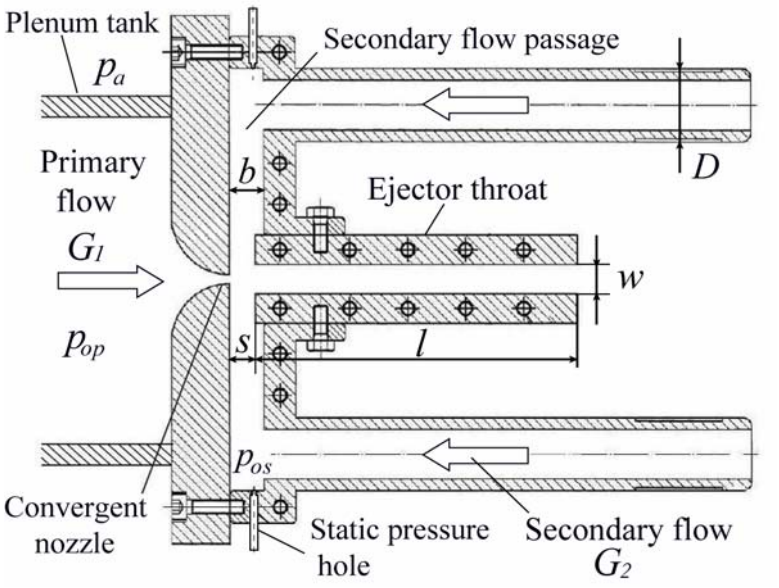


**Fig. 1. The ejector model in this study**

## EXPERIMENT

### Experimental Apparatus

The piping system and the apparatus in this experiment are shown in Fig. 2. High pressure air is generated by two compressors and pass through an air dryer, a surge tank, an oil mist separator and an oil removal filter. The compressed air is supplied into the plenum tank attached to the convergent nozzle. The stagnation pressure in the plenum tank $p_{op}$ can be adjusted manually by controlling two air release valves and $p_{op}$ is measured by digital manometer. In the experiment the ratio of stagnation pressure of the primary jet $p_{op}$ to atmospheric pressure $p_a$, *NPR*, is changed from 1.893 to 4.00. Two cases are tested, i.e. there is the secondary flow rate $G_2 \neq 0$ and $G_2 = 0$. The secondary flow rate $G_2$ is changed by varying *s/d* to clarify how the change of the secondary flow influences the internal flow of the ejector and when there is not secondary flow, it may be understood to be the flow pattern in the vacuum ejector. The valve is installed on the pipe upstream of, and connected to the secondary flow passage, to examine the flow behavior when it is open ($G_2 \neq 0$) or closed ($G_2 = 0$).

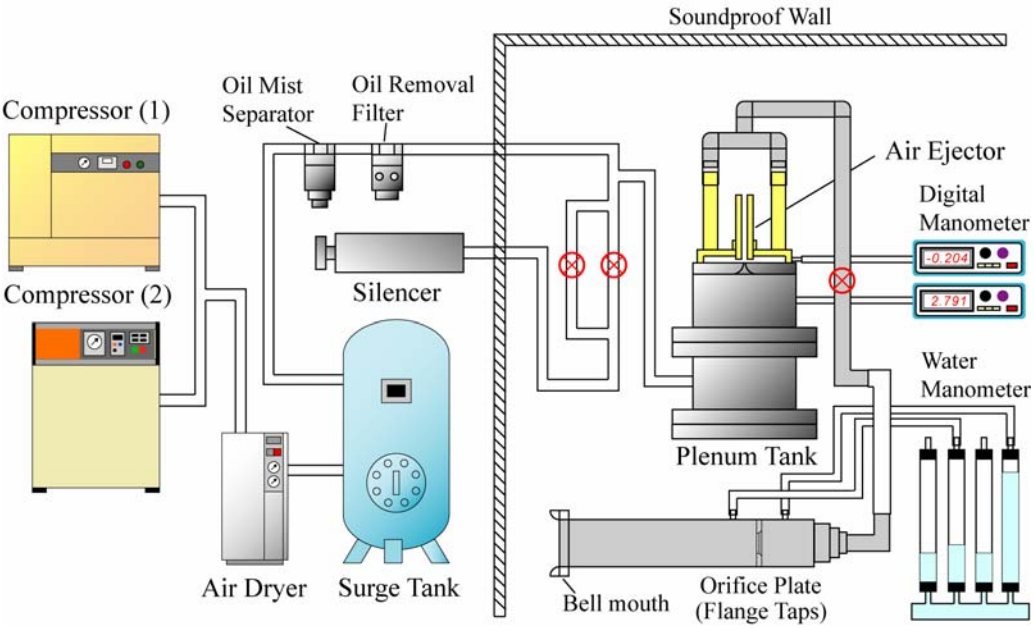


**Fig. 2. Experimental arrangement**

### Optical System

Shadowgraph and schlieren methods are employed to visualize the internal flow of the ejector. The light source is a Xenon discharge tube with duration of 180 ns. This light is made parallel with two parabolic mirrors whose diameter is 150 mm and focal length is 750 mm. In schlieren method the knife-edge is placed perpendicular and parallel to the jet axis to obtain the density gradient in each direction.

### Measurement of Stagnation Pressure and Flow Rate of the Secondary Fluid

The air in the secondary flow passage is almost stagnant, so that the pressure measured through the static hole in Fig. 1 is stagnation pressure of the secondary flow which can be used to examine the ejector effect and vacuum performance. The measurement of pressure is made four times by digital manometer which is $\pm 0.1$ % error margin and its averaged value is represented by $p_{os}$. The secondary flow rate $G_2$ is measured with orifice flow meter according to JIS Z 8762 (Japanese Industrial Standard). The diameter of the pipe on which the orifice plate is installed is 51 mm and the bell mouth whose radius of the wall curvature is 20 mm is attached to the entrance to the pipe. Arrangement of flange pressure taps with water monometer is employed to measure the differential pressure and the mass flow rate of the secondary flow $G_2$ is obtained. When the visualization study and measurement of the ejector performance are made, the orifice plate is removed because the pressure drop across the orifice might affect the flow field in the ejector.

## RESULTS AND DISCUSSION

### Stagnation Pressure and Flow Rate of the Secondary Fluid

Figure 3 is a plot of the stagnation pressure in the secondary flow passage normalized by the atmospheric pressure $p_{os}/p_a$ against the nozzle pressure ratio $p_{op}/p_a$ ($NPR$) for varying port breadths divided by nozzle height $s/d$. The value of $p_{os}/p_a$ may be a measure of the ejector effect and the vacuum performance. In Fig. 4 the secondary flow rate $G_2$ is exhibited against the pressure ratio $p_{op}/p_a$ for each $s/d$. At all of $s/d$ 's, Fig. 4 shows that the maximum flow rate occurs at $NPR = 3.10$ where the lowest stagnation pressure is obtained as shown in Fig. 3. At pressure ratios higher than $NPR = 3.10$, $G_2$ decreases with increase in $NPR$. When $G_2 = 0$, there is little difference in $p_{os}/p_a$ at all of $s/d$ 's, and thus, the vacuum performance does not depend on the port breadth $s$. The value of $p_{os}/p_a$ is the lowest at $NPR = 3.70$, the vacuum performance being the highest independent of port breadth.

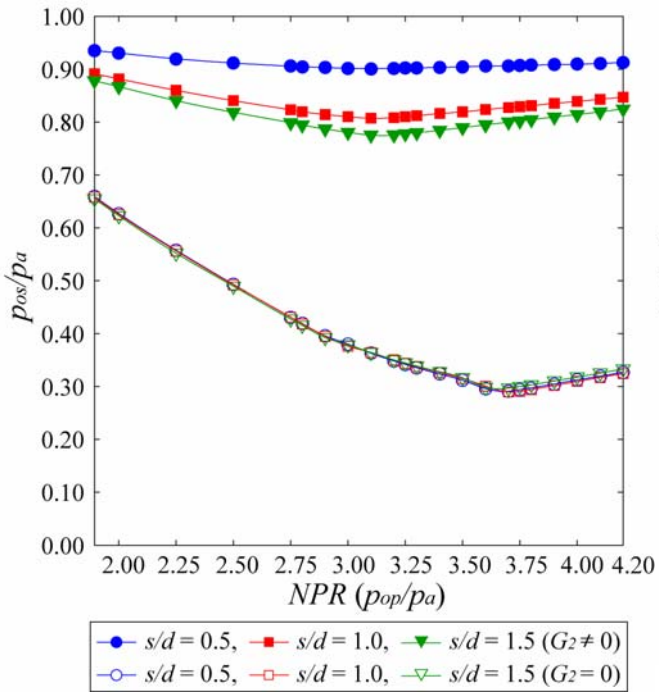


**Fig. 3. $p_{os}/p_a$ vs $NPR$ for $s/d$ in $G_2 \neq 0$ and $G_2 = 0$**

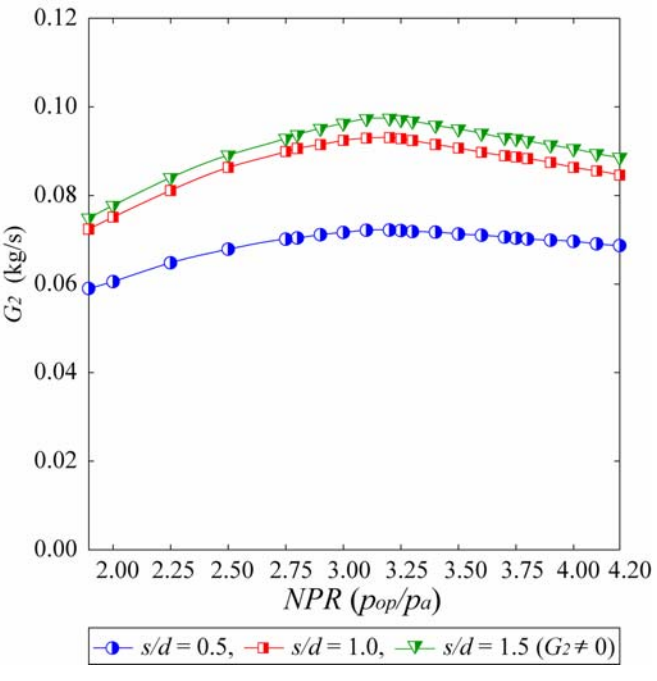


**Fig. 4. $G_2$ vs $NPR$ for $s/d$ in $G_2 \neq 0$**

**Visualization in the Internal Flow of the Ejector**

*Flow Behavior When There is Secondary Flow Rate*

Figures 5, 6 and 7 show shadowgraph pictures of the internal flow field of the ejector for *s/d* = 0.5, 1.0 and 1.5, respectively, at each $NPR$. The secondary fluid enters the mixing chamber through the shear action at the boundary between the primary and secondary streams. When $NPR$ exceeds a critical value ( $NPR$ = 1.893), the primary flow is choked and underexpanded. In such a flow field the expansion wave is generated at the nozzle lip and it reaches the jet boundary where compression wave is reflected. The compression wave reaches the jet boundary and is reflected from it as expansion wave, such wave reflection repeats itself and as a result the cellular structure of the jet is formed. It is found that the internal flow has some different flow patterns at each range of *NPR*. As shown in Figs. 3 and 4, the stagnation pressure of the secondary flow and the secondary flow rate $G_2$ at *s/d* = 0.5 differs much from those at *s/d* = 1.0 and 1.5. Thus, the flow patterns at *s/d* = 0.5 are discussed first, and then, those at *s/d* = 1.0 and 1.5 are discussed.

*Flow Behavior in the Ejector at s/d =0.5*

Figures 5(a) to 5(f) show some of the typical shadowgraph pictures of the internal flow of the ejector at varying nozzle pressure ratios *NPR*. At *NPR* = 1.893 to 2.00, the secondary fluid is drawn by the primary flow. The impingement of the secondary flow on the jet boundary of the first cell makes the jet boundary narrow. Pressure outside of the jet flow increases owing to the ejected secondary fluid and the velocity decreases, and then downstream the fist cell structure collapses. At *NPR* = 2.25 to 2.50 the strength of the expansion and compression waves in the primary jet increases with increase in *NPR* and the jet boundary of the first cell expands. Secondary flow rate increases because of the increase of shearing action. The boundary of the second cell is narrowed due to increase in the flow rate of the secondary fluid. The typical flow pattern at *NPR* = 2.50 is shown in Fig. 5(b). When the nozzle pressure ratio is higher at *NPR* = 2.75 to 2.80, the compression wave in the primary jet becomes stronger and the oblique shock forms. These oblique shock waves are reflected in the jet boundary and the second cell is formed. At higher nozzle pressure ratio the oblique shock becomes stronger. Further downstream a train of shocks can be seen, proving that cellular structure is formed. At *NPR* = 2.90 to 3.00, the secondary flow, when it comes out of the port, is separated at the corner and then reattached on the ejector wall. When this reattachment occurs, the boundary of the separated flow is concaved, resulting in the generation of compression wave. The compression wave interferes with the shock in the primary jet as shown in Fig. 5(d). This compression wave strengthens the oblique shock in the primary jet even more. When *NPR* = 3.10 as shown in Fig. 5(e), the oblique shock wave in the first cell which is stronger now due to the interference with the stronger compression wave from the separated shear layer. Further downstream at the end of the first cell another oblique shock wave appears, which is the result of the merging of the compression wave at the boundary layer of the secondary flow along the wall. At *NPR* = 3.20 to 4.20 the oblique shock in the primary jet becomes strong and reaches the turbulent boundary layer on the wall from which it is reflected, its reflection being repeated as it flows downstream as can be seen in Fig. 5(f). Therefore, the pressure increases downstream and velocity decreases as the air passes through each oblique shock wave. When the oblique shock wave is reflected from the boundary layer, Mach reflection occurs and the pressure rises behind the Mach stem. This pressure rise propagates upstream through the boundary layer and reaches the slot where the secondary fluid issues. Thus, the pressure at the exit of the secondary fluid increases to some extent, resulting in the reduction of the flow rate. So, the secondary flow rate decreases under such flow conditions, which explains the curves shown in Fig. 4 where the maximum flow rate is obtained at *NPR* = 3.10.

*Flow Behavior in the Ejector at s/d = 1.0 and 1.5*

As shown in Fig. 3 and 4, when the port size is large, the secondary flow increases, so that shearing action between the primary and secondary fluids becomes more active. At *NPR* = 1.893 to 2.00, as shown in Figs. 6(a) and 7(a), the boundary of the primary jet is narrowed because the mass flow of the secondary fluid is large and when *NPR* = 2.25 to 2.50, the boundary of the second cell is narrowed more and the cell becomes longer downstream than at *s/d* = 0.5. The cellular structure is generated further downstream and the bow shock waves occur. As the nozzle pressure ratio increases, the secondary flow rate increases and the oblique shock appears clearly in the primary jet. At *NPR* = 2.75 to 2.80 for *s/d* = 1.0 and at *NPR* = 2.75 to 3.00 for *s/d* = 1.5, compression waves in the first cell become an oblique shock wave and a train of oblique shocks follow. When *NPR* = 2.90 to 3.00 for *s/d* = 1.0 and at *NPR* = 3.00 for *s/d* = 1.5, compression wave originates near the separated boundary layer from the corner of the port, and it grows into a shock at the boundary of the primary jet. When *NPR* = 3.10 for *s/d* = 1.0 and *s/d* = 1.5, the weak compression wave can be seen at a point of intersection of the oblique shock and the jet boundary in Figs. 6(e) and 7(e). This compression wave can be considered to occur due to the separation of the developed boundary layer along the wall. At higher *NPR* the oblique shock becomes stronger and it reaches the boundary layer on the wall as shown in Fig. 6(f) (*s/d* = 1.0, *NPR* = 4.00), where Mach reflection seems to occur, so that the normal shock, or Mach stem stands near the wall. This flow situation makes the secondary flow rate lower. The similar flow conditions are obtained for the flow field for *s/d* = 1.5 at *NPR* = 3.20 to 4.20 as shown in Fig. 7(e).

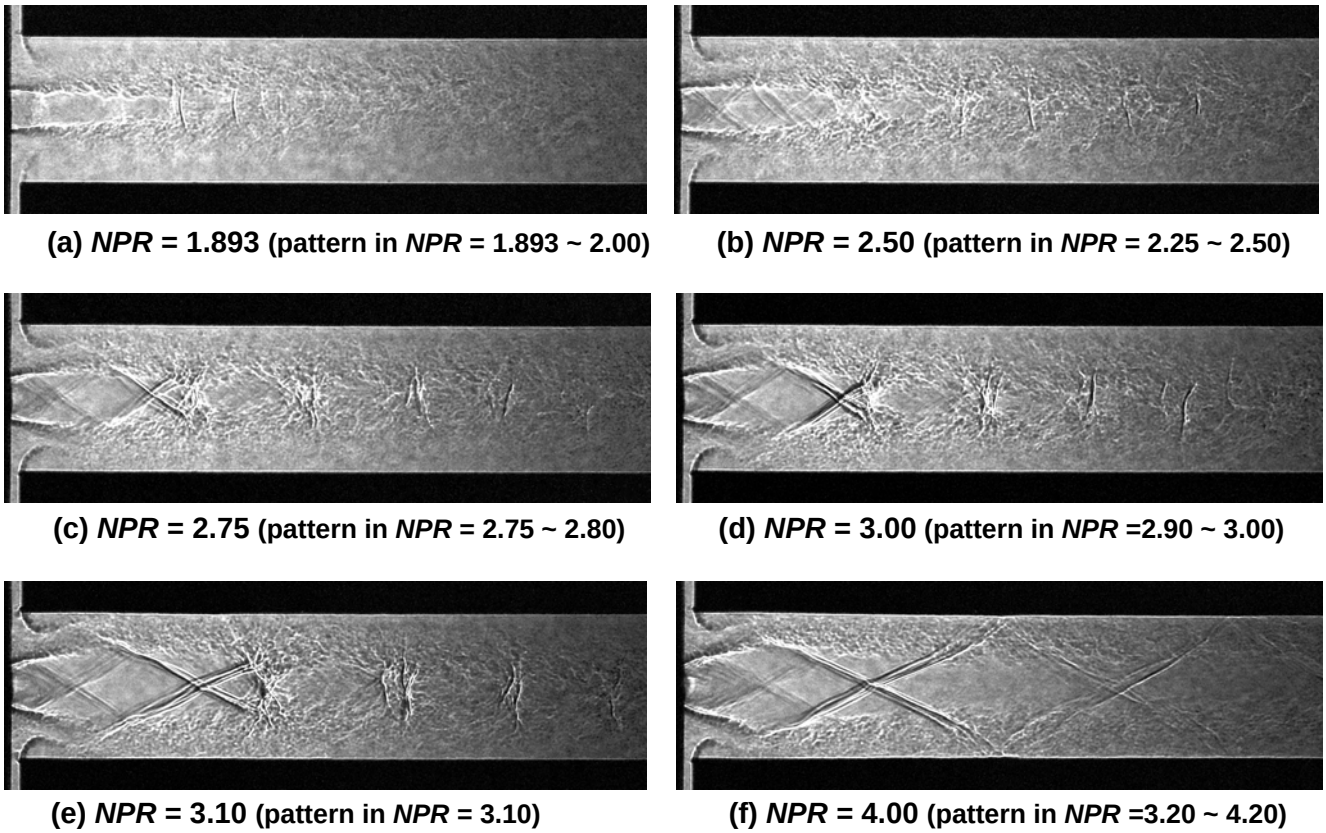

**(a) *NPR* = 1.893 (pattern in *NPR* = 1.893 ~ 2.00)** **(b) *NPR* = 2.50 (pattern in *NPR* = 2.25 ~ 2.50)**

**(c) *NPR* = 2.75 (pattern in *NPR* = 2.75 ~ 2.80)** **(d) *NPR* = 3.00 (pattern in *NPR* =2.90 ~ 3.00)**

**(e) *NPR* = 3.10 (pattern in *NPR* = 3.10)** **(f) *NPR* = 4.00 (pattern in *NPR* =3.20 ~ 4.20)**

**Fig. 5. Shadowgraph pictures ($G_2 \neq 0$, *s/d* = 0.5)**

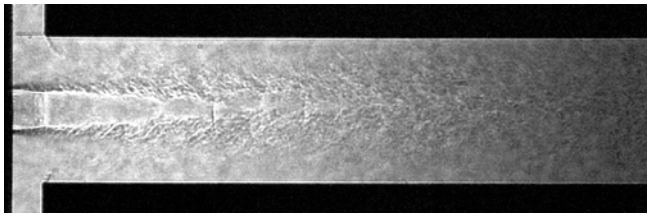

**(a) *NPR* = 1.893 (pattern in *NPR* = 1.893 ~ 2.00)**

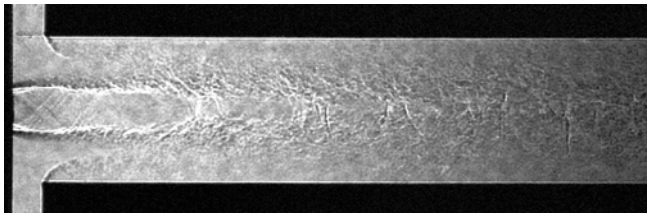

**(b) *NPR* = 2.50 (pattern in *NPR* = 2.25 ~ 2.50)**

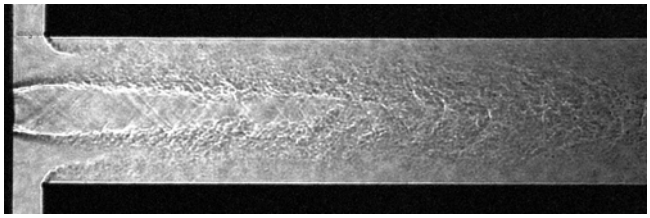

**(c) *NPR* = 2.75 (pattern in *NPR* = 2.75 ~ 2.80)**

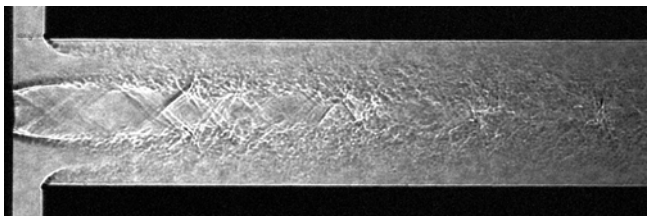

**(d) *NPR* = 3.00 (pattern in *NPR* =2.90 ~ 3.00)**

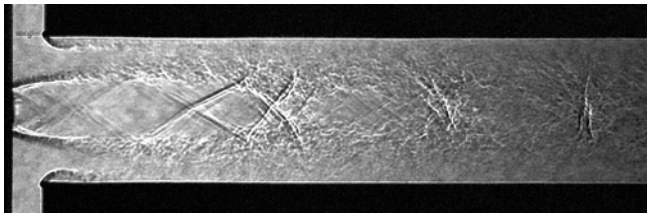

**(e) *NPR* = 3.10 (pattern in *NPR* = 3.10)**

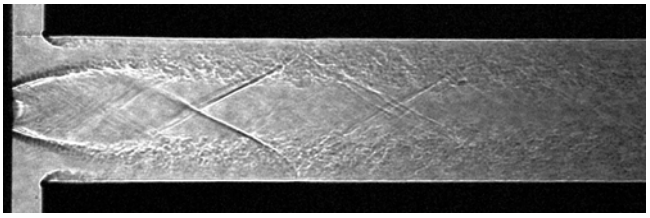

**(f) *NPR* = 4.00 (pattern in *NPR* =3.20 ~ 4.20)**

**Fig. 6. Shadowgraph pictures ($G_2 \neq 0$, *s/d* = 1.0)**

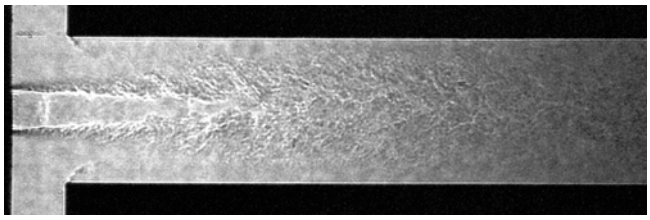

**(a) *NPR* = 1.893 (pattern in *NPR* = 1.893 ~ 2.00)**

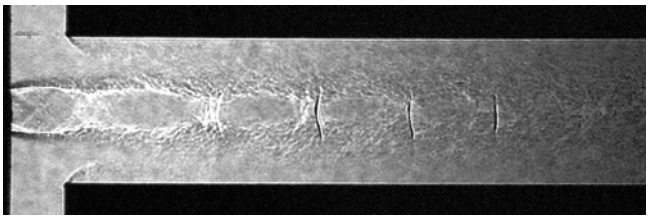

**(b) *NPR* = 2.50 (pattern in *NPR* = 2.25 ~ 2.75)**

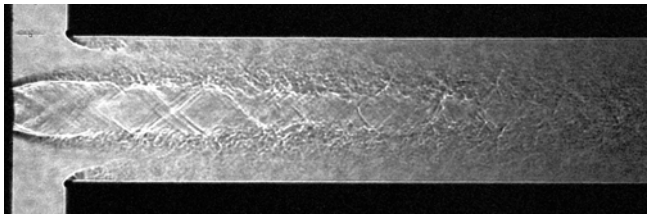

**(c) *NPR* = 3.00 (pattern in *NPR* = 2.80 ~ 3.00)**

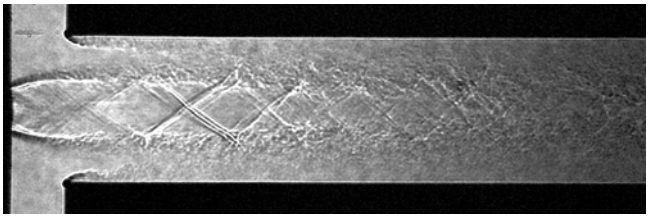

**(d) *NPR* = 3.10 (pattern in *NPR* = 3.10)**

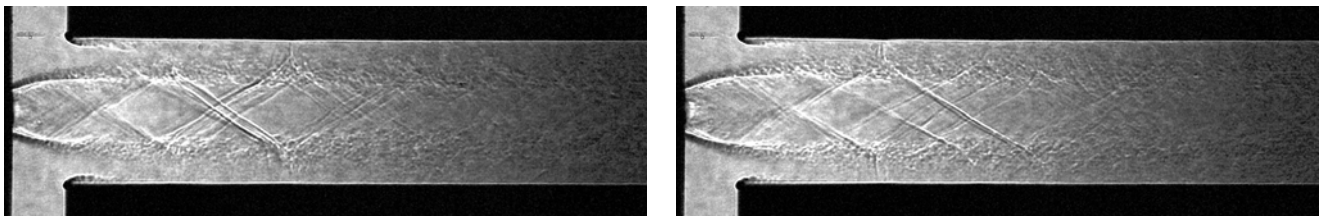

**(e) *NPR* = 3.40 (pattern in *NPR* = 3.20 ~ 3.40)** **(f) *NPR* = 4.00 (pattern in *NPR* =3.50 ~ 4.20)**

**Fig. 7. Shadowgraph pictures ($G_2 \neq 0$, *s/d* = 1.5)**

*Flow Behavior When There is No Secondary Flow Rate*

As shown in Fig. 3, data for stagnation pressure $p_{os}/p_a$ vs *NPR* for different port sizes fall on a single curve, when there is no secondary flow rate, i.e. performance of the vacuum ejector does not depend on the port breadth. The visualization study reveals that the flow patterns of internal flow are the same irrespective of the port breadth. Therefore, only the flow patterns obtained at *s/d* = 1.0 are shown below and discussed. The underexpanded jet of the primary fluid in the vacuum ejector can be said generally to expand more than the free jet because of the presence of low pressure region near the nozzle exit. At *NPR* = 1.893 to 2.00, an underexpanded jet can be seen in the ejector as in Fig. 8(a). Compression wave in the underexpanded jet grows into an weak oblique shock which reaches the end of the first cell as shown in Fig. 8(b) when *NPR* = 2.25 to 2.50. At *NPR* = 2.75 to 2.80 the compression wave and shock wave grow in strength and Mach disk forms in the first cell. The reflected shock interferes with the jet boundary and expansion wave is reflected, resulting in the formation of the second cell of the jet. Further downstream weak bow shock occurs and behind it the cellular structure disappears. When nozzle pressure ratio *NPR* = 2.90 to 3.00, strong Mach disk appears as shown in Fig. 8(d) and in the flow field behind it the flow is subsonic. At higher nozzle pressure ratio *NPR* = 3.10 to 3.60, the Mach disk becomes stronger and slip line originating from the triple point can be seen. The reflected shock from the triple point is reflected from the wall boundary layer, and then, reflected from the slip line, the repetition of this wave being continued along the wall and in the repetition the Mach reflection can occur. At *NPR* = 3.70 as shown in Fig. 8(f), the oblique shock wave which originates from the concaved streamline near the wall is strong because of the high Mach number in front of it and it makes Mach disk small. Another shock wave is generated from the boundary layer on the wall, which interferes with the reflected shock from the triple point, resulting in the another Mach disk, so that the flow behind this shock system is almost entirely subsonic. At *NPR* = 3.75 to 4.00, Mach disk disappears, and the oblique shock originated at the concaved jet boundary reaches the boundary layer on the wall, where the boundary layer is separated and another oblique shock appears. As a result the boundary layer becomes thick and the main flow passage becomes narrow. At *NPR* = 4.10 to 4.20 all shock waves in the entire flow field shown in the figure are oblique, which occur with the turbulent boundary layer separation and this flow pattern repeats itself downstream, thus the flow being entirely supersonic.

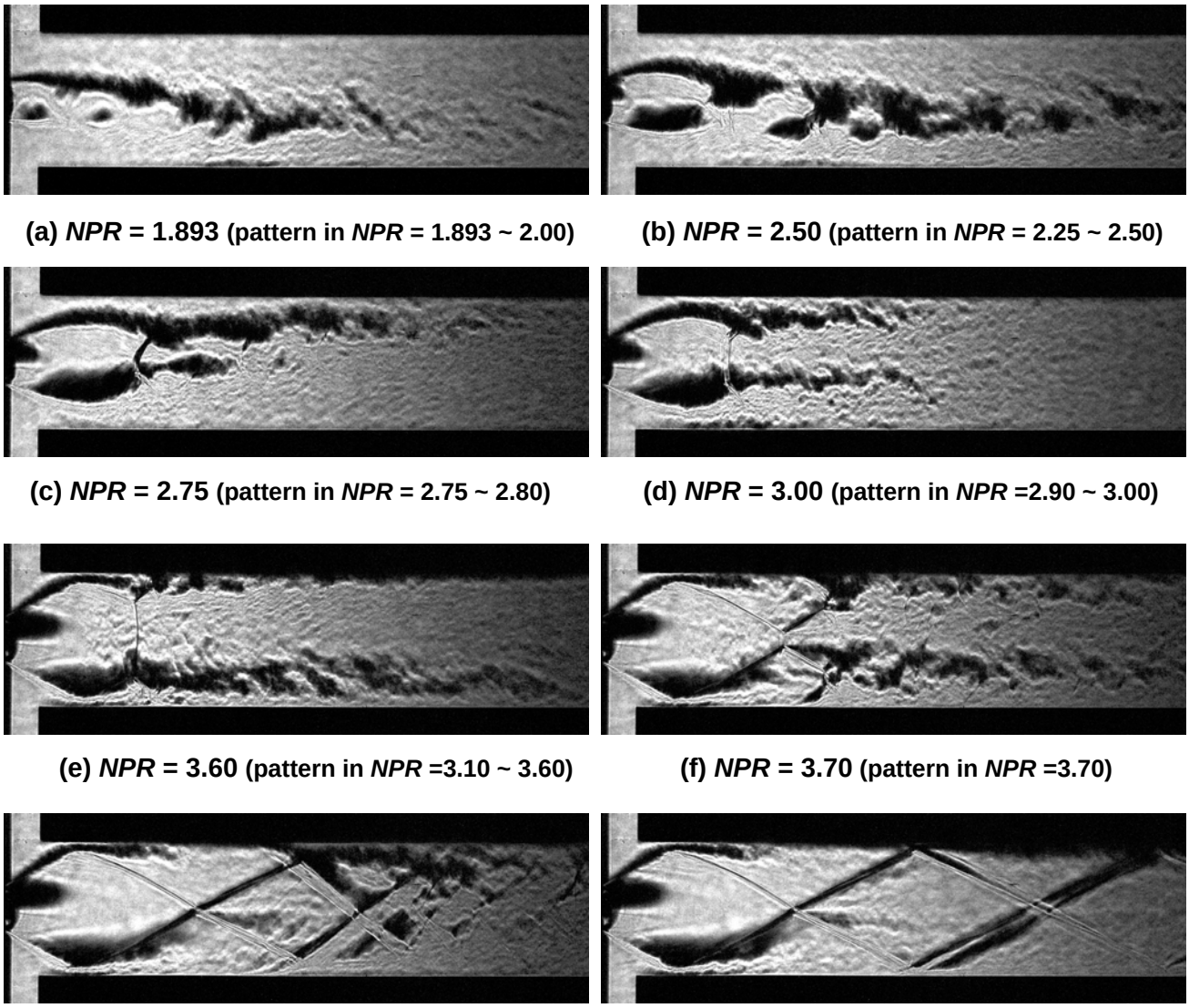

**(a) *NPR* = 1.893 (pattern in *NPR* = 1.893 ~ 2.00)** **(b) *NPR* = 2.50 (pattern in *NPR* = 2.25 ~ 2.50)**

**(c) *NPR* = 2.75 (pattern in *NPR* = 2.75 ~ 2.80)** **(d) *NPR* = 3.00 (pattern in *NPR* =2.90 ~ 3.00)**

**(e) *NPR* = 3.60 (pattern in *NPR* =3.10 ~ 3.60)** **(f) *NPR* = 3.70 (pattern in *NPR* =3.70)**

**(g) *NPR* = 3.80 (pattern in *NPR* = 3.75 ~ 4.00)** **(h) *NPR* = 4.20 (pattern in *NPR* =4.10 ~ 4.20)**

**Fig. 8. Schlieren pictures ($G_2 = 0$, *s/d* = 1.0)**

*The Relationship between The Internal Flow and Performance of Ejector*

Figures 9 to 11 show schlieren pictures of the internal flow of the ejector at *NPR* = 3.10 for *s/d* = 0.5, 1.0 and 1.5, respectively, where the secondary flow rate $G_2$ is the highest and the stagnation pressure $p_{os}/p_a$ is the lowest as shown in Figs. 3 and 4. For all of *s/d* = 0.5, 1.0, 1.5, the compression wave occurs at the separated shear layer and at a point of intersection of the oblique shock and the jet boundary, resulting in the generation of oblique shock wave and it is considered that the velocity of the secondary fluid upstream of the oblique shock is high. At higher nozzle pressure ratios than *NPR* = 3.10, the entire flow field is governed by the oblique shock waves, and thus, the pressure of the secondary flow near the port is higher and its velocity lower, resulting in the lower flow rate and higher stagnation pressure of the secondary flow.

Figures 12 shows the schlieren pictures of the internal flow of the ejector for *s/d* = 1.0. When there is no secondary flow rate $G_2$ at *NPR* = 3.70, the vacuum performance is highest as shown in Fig.3. This oblique shock wave interferes with the wall turbulent boundary layer on the other side and then another oblique shock wave is reflected from the wall. Since the angle of this shock wave against the central axis is the largest at all of *NPR*'s, the velocity being high and the pressure low upstream of the shock wave, it follows that the highest vacuum is obtained in the secondary flow.

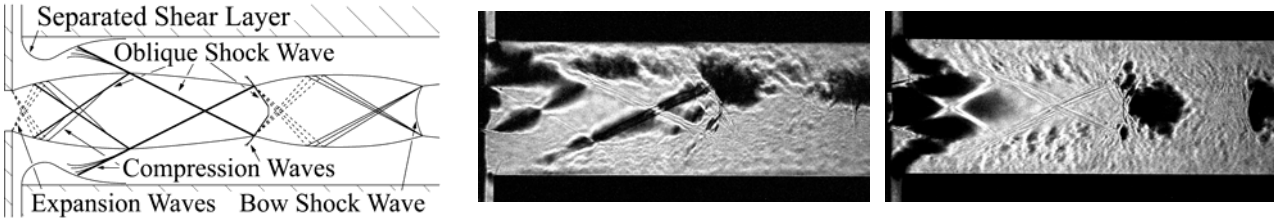


**Fig. 9. Pattern diagrams and Schlieren pictures when there is $G_2$ at *s/d* = 0.5**

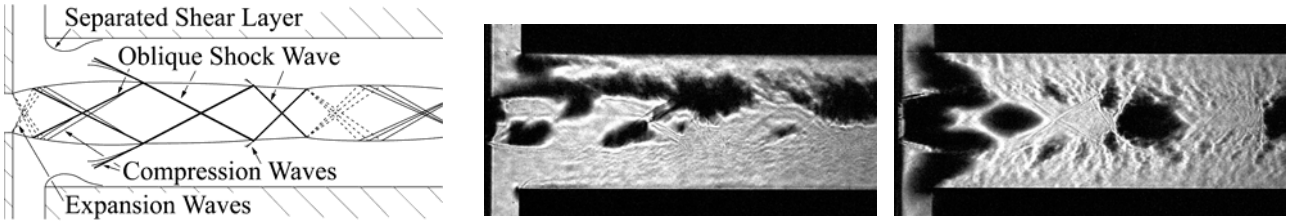


**Fig. 10. Pattern diagrams and Schlieren pictures when there is $G_2$ at *s/d* = 1.0**

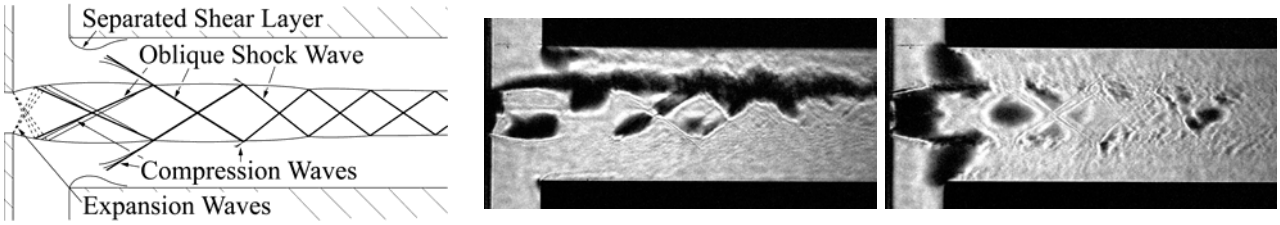


**Fig. 11. Pattern diagrams and Schlieren pictures when there is $G_2$ at *s/d* = 1.5**

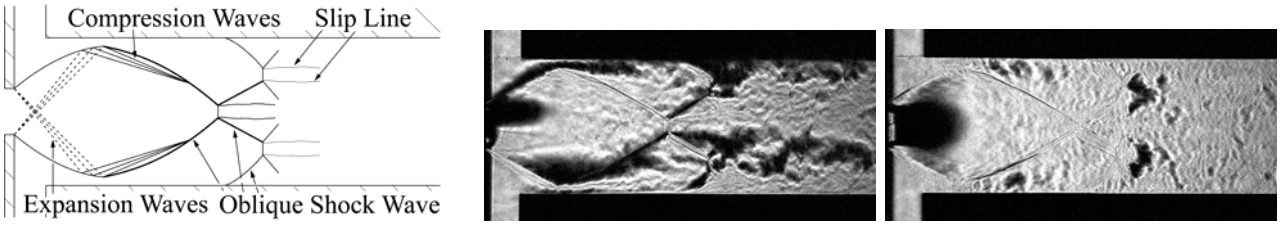


**Fig. 12. Pattern diagrams and Schlieren pictures when there is not $G_2$ at *s/d* = 1.0**

## CONCLUSIONS

To clarify the flow behavior inside a simple model of ejector with the convergent nozzle, the internal flow of the ejector is visualized and the ejector performance is investigated by measuring the stagnation pressure of the secondary flow. As a result, conclusions are drawn as follow;

(1) The ejector effect is highest at *NPR* = 3.10 for all *s/d*'s.

(2) When there is secondary flow $G_2 \neq 0$, the internal flow of the ejector can be divided into three flow patterns. First pattern is the underexpanded jet of the primary fluid whose boundary is narrowed by the impingement and shearing action of the secondary flow. Second pattern is that the oblique shock of the first cell interferes with the separated shear layer. Third pattern is that the oblique shock interferes with the wall boundary layer downstream.

(3) When the oblique shock wave of the first cell interferes with the separated shear layer and at a point of intersection of the oblique shock and the jet boundary, the highest ejector effect is obtained.

(4) The vacuum performance does not depend on the port breadth and is the highest at *NPR* = 3.70.

(5) When there is no secondary flow $G_2 = 0$, the internal flow takes three patterns with increase in *NPR*, i.e. the underexpanded jet, the flow with the normal shock wave and with the oblique shock wave.

(6) When the angle of the oblique shock wave which is generated from the wall turbulent boundary layer is the largest, the highest vacuum performance is obtained.


## ACKNOWLEDGMENT

The experiments described above were made in cooperation with Messrs. T. Yoneyama. The authors would like to thank his assistance.


## REFERENCES


M. Endo, Y. Sakakibara and J. Iwamoto (2005), "Behavior of Internal Flow in Air-Driven Vacuum Ejector (Flow Analysis using Hydraulic Analogy), " The 8TH International Symposium on Fluid Control, Measurement and Visualization, 383.

J. Kastner and J. R. Spooner (1950), "An investigation of the performance and design of the air ejector employing low pressure air as the driving fluid, " Proc. Instn Mech. Engrs, Vol.162, pp. 149-159.

K. Matsuo, *et al*. (1982), "A Study on Supersonic Air Ejector (2nd Report)", pp. 648-650.

K. Tani, K. Kato and S. Hasegawa (2007), "Flow Visualization in an Ejector-Jet Mode of Combined Cycle Engine, " Aerospace numeric simulation technology symposium, pp. 379-381.

I. Watanabe, and T. Watanabe (1956), "Experimental Study on Pneumatic Air Ejector (3rd and 4th Report), " pp. 600-601.

E. Yamada, and H. Nishijima (2008), "Ejector system for small truck refrigerators, " JSAE Annual Congress (spring) Proceedings, No. 48-08, pp. 5-8.

## APPENDIX I. NOTATION

$p_a$ Atmosphere pressure [atm]

$p_{op}$ Stagnation pressure of plenum tank [atm]

$p_{os}$ Stagnation pressure of secondary flow's tank [atm]

*NPR* Pressure ratio between plenum chamber and atmosphere

$d$ Convergent nozzle width [mm] ($d$ = 3 mm)

$s$ Port breadth [mm] ($s/d$ = 0.5, 1.0, 1.5)

$w$ Throat width [mm] ($w$ =10 mm, $w/d$ = 3.33)

$l$ Throat length [mm] ($l + s$ = const = 120 mm)

$D$ Vacuum hole diameter of secondary flow [mm] ($D$ = 18 mm)

$b$ Bread of secondary flow passage[mm] ($b$ = 12 mm)

$G_1$ Primary flow [kg/s]

$G_2$ Secondary flow [kg/s]